Journal of Renewable Materials

Tech Science Press

Doi:10.32604/jrm.2025.02024-0073

ARTICLE

Development of Flame Retardant Composite Based on Glucose-Citric Acid-Based Resin Reinforced by Walnut Shell Powder

Zhenzhou Wang[1], Rui Luo[1], Wenqing Yang[1], Seng Hua Lee[2,*], Wei Chen Lum[3], Longjiang Liu[4], Xiaojian Zhou[1] and Jun Zhang[1,*]

[1]Yunnan Provincial Key Laboratory of Wood Adhesives and Glued Products, Southwest Forestry University, Kunming, 650224, China
[2]Department of Wood Industry, Faculty of Applied Sciences, Universiti Teknologi MARA Pahang Branch Jengka Campus, Bandar Tun Razak, 26400, Pahang, Malaysia
[3]Department of Bio and Natural Resource, Faculty of Bioengineering and Technology, Universiti Malaysia Kelantan, Jeli, 17600, Kelantan, Malaysia
[4]School of Chemical Engineering, Yunnan Vocational College of National-Defense Technology, Yunnan Open University, Kunming, 650223, China

*Corresponding Authors: Seng Hua Lee. Email: leesenghua@uitm.edu.my; Jun Zhang. Email: zj8101274@163.com

Received: 26 December 2024; Accepted: 27 February 2025; Published: 23 June 2025

ABSTRACT: Highly flame-retardant bio-based composites were prepared in this study. Firstly, glucose-citric acid (GC) resin was synthesized through the interaction of glucose and citric acid derived from agricultural and forestry sources. Polyvinyl alcohol (PVA) served as a toughening agent, whereas walnut shell powder (WSP) functioned as a filler in the formulation of a thermosetting bio-based GC-PVA-WSP (GCPW) composite with GC resin. The findings demonstrated that boric acid increased the limited oxygen index (LOI) value of GCPW to 33%, while simultaneously diminishing its total smoke production (TSP) by 99.9%, and achieving a flame retardant index (FRI) of 5.04. In addition, the incorporation of WSP enhanced the compressive strength of the GCPW composite to 9.15 MPa. Concurrently, the GCPW composite demonstrates excellent hydrophobic properties, with a thermal conductivity as low as 0.086 W/m·K.

KEYWORDS: Glucose; citric acid; walnut shell powder; flame retardant; bio-based composite

1 Introduction

The fabrication of composites derived from renewable and biodegradable resources is an effective approach to mitigating environmental pollution and promoting sustainable industrial advancement [1,2]. These composites not only possess the excellent properties of traditional petroleum-derived composites, such as high mechanical strength and light weight [3,4], but more importantly, they have characteristics such as renewability, degradability, and low toxicity [5,6], which are crucial for reducing environmental pressure and promoting sustainable development.

Citric acid serves as a promising chemical for wood modification and as an eco-friendly wood binder [7]. Nonetheless, the sole application of citric acid may be insufficient. Consequently, citric acid is frequently combined with other chemicals to augment its efficacy [7]. For instance, citric acid has been reacted with sucrose, a disaccharide, to enhance the bonding efficacy of citric acid as a binding agent for wood composites [8]. Li et al. [9] projected that the reaction between citric acid and glucose, a monosaccharide, is anticipated to be simpler than the reaction between sucrose and citric acid, potentially yielding a good binder.

Glucose, a significant biomass material prevalent in plants, is the main product of plant photosynthesis [10,11] and has the advantages of wide sources and simple processing. At the same time, glucose molecules contain multiple hydroxyl groups and have good reactivity [12]. They can be used to prepare non-toxic and biodegradable materials in conjunction with other materials through chemical reactions or physical blending [13–16]. Citric acid and glucose, via an esterification process, have been utilized as an efficient plywood adhesive and demonstrated outstanding performance [9]. However, the resin has a low solid content and high brittleness after curing, which severely restricts its application [17].

Aside from its application as a binding agent, research on the synthesis of glucose-citric acid composites is quite limited. Furthermore, due to their biodegradability, it is expected that the strength of composites derived from citric acid and glucose needs enhancement. Therefore, polyvinyl alcohol (PVA) is proposed. PVA, being a non-toxic and biodegradable material, is widely used to prepare films with good toughness [18–20]. PVA serves as a toughening agent when combined with glucose and citric acid to produce resilient GCP composites.

In addition, the rapid growth of biomass waste generation has emerged as a major global challenge [21], with the volume of discarded walnut shells increasing year by year [22]. Walnut shells contain a high amount of lignin and exhibit good fluidity, keratin content, low price and density [23,24]. Walnut shell powder (WSP) can be blended with GCP composite as a filler to reduce the amount of GCP resin required, lower preparation costs, and improve the strength of the composite, thereby alleviating the problem of waste disposal of walnut shells. WSP has often been used as a reinforcing agent for polymeric composite to enhance their mechanical strength [25]. Their good toughness and dispersibility can enhance the strength of the polymer blends. WSP has also been added into the polyurethane foam as a filler to improve its flame retardancy and thermal stability [26]. However, its effects as a filler in the glucose-citric acid based composite aremains unexplored and worth investigation. To further improve the flame retardancy of the composites, boric acid can be employed [27]. Boric acid is a common flame retardant widely used in blending with polymer resins to improve the flame retardancy of the blends [28–30].

Despite glucose and citric acid being recognized as sustainable precursors, their application in the development of flame-retardant biocomposites remained infrequently explored. Based on the above viewpoints, this study utilized glucose and citric acid to prepare GC resin through an esterification condensation reaction. Then, a flame-retardant thermosetting composite material with high compressive strength was prepared by blending it with PVA, WSP, and boric acid. It is hypothesized that the strength of the GC composite could be enhanced by PVA and WSP while boric acid will synergistically enhance its flame-retardant properties.

2 Materials and Methods

2.1 Materials

The glucose (99%) and citric acid (99.5%) used in this study were produced and purchased from McLean Biochemical Technology Co., Ltd. (Shanghai, China), polyvinyl alcohol (PVA) was purchased from Yousuo Chemical Technology Co., Ltd. (Jinan, China), which was produced by Wanwei High tech Materials Co., Ltd. (Chaohu, China) and boric acid was purchased from Xilong Chemical Co., Ltd. (Chengdu, China), which was produced by Xilong Chemical Co., Ltd. (Chengdu, China). Walnut shell powder (WSP, 200 mesh) was produced and obtained from Fenyang Sunshine Industrial Co., Ltd. (Fenyang, China), which mainly consists of peach quinone (40%), glucoside (30%) and tannin (20%). Potassium dichromate was produced and purchased from Fengchuan Chemical Reagent Technology Co., Ltd. (Tianjin, China).

2.2 Preparation of GCPW Composites

Fifteen grams of glucose and fifteen grams of citric acid were combined to produce GC resin. At the same time, 40 g of water and 15 g of PVA were added into a 250 mL beaker, the DF-101S magnetic stirrer was used to dissolve PVA at 80°C. Subsequently, a 20% PVA solution was added into the beaker containing GC resin and stirred well to obtain GCP resin. Then, boric acid powder was mixed with GCP resin to obtain the GCP1 and GCP2 resins. Both resins were then cooled at room temperature, respectively. Afterwards, 18 g of WSP was mixed with each cooled resin. Subsequently, each mixture was injected into a mold and subjected to an oven temperature of 70°C for 36 h. The sample was heated to 120°C for 24 h and then allowed to cool to room temperature, resulting in a GCPW composite. In addition, under the same conditions, without adding PVA, GC -WSP (GCW) composite was prepared for comparison with GCPW composite. The specific material dosage and formulation are shown in Table 1, while the preparation process is illustrated in Scheme 1.

Table 1: Formulas of different GC resin-based composites

Sample	Resin	Glucose (g)	Citric acid (g)	Polyvinyl alcohol (g)	Boric acid (g)	Walnut shell powder (g)
GCW	GC	15	15	/	/	18
GCPW	GCP	15	15	15	/	18
GCPW1	GCP1	15	15	15	2	18
GCPW2	GCP2	15	15	15	4	18

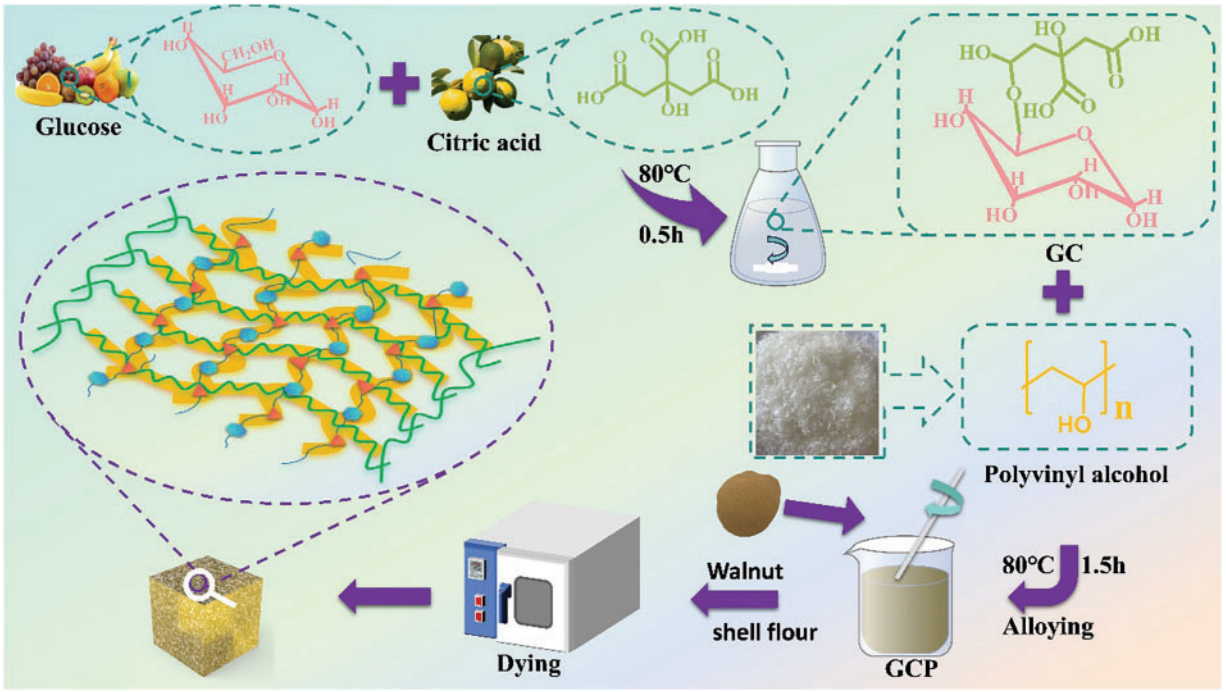

Scheme 1: Preparation process of GCPW1 composite

2.3 Characterizations

All composites produced in the study were stored in a conditioning room for 24 h to attain a constant mass.

2.3.1 Chemical Analysis

The samples were tested using a a Varian-1000 infrared spectrometer. The composite material was grounded into powder with a particle size of 35–38 μm using a JMS16A crusher. 0.01 g of powder were taken from each solid sample, 1 g of KBr was mixed with the test sample, and the wavelength from 500–4000 cm^{-1} was used to scan the sample. A Bruker 400 MHz nuclear magnetic resonance spectrometer with a collection time of 3.0 s was used. Meanwhile, an X-ray diffractometer (XRD-7000) was used to obtain the X-ray signal characteristics of the measured sample after diffraction to obtain the crystal structure. The X-ray photoelectron spectrometer was used as per literature [31].

2.3.2 Morphology

The internal structure of the composites was observed using a S4800 scanning electron microscopy.

2.3.3 Apparent Density, Pulverization Rate, and Compressive Strength

The apparent density measurement of the sample was carried out according to ASTM-D162208-2008. The pulverization rate was calculated based on the quantity of leftovers of the composite. The compressive strength test was conducted.

2.3.4 Wettability and Dimensional Stability

The Datphysical DCAT 21 instrument was employed to assess the contact angle. The composite were tested for expansion and water absorption.

2.3.5 Thermogravimetric Analysis (TGA), Thermal Conductivity, Limit Oxygen Index (LOI) and Thermogravimetric Analysis-Infrared Spectroscopy (TGA-IR) Testing

The 209 F3 thermogravimetric analyzer was used to test the mass loss of composite in response to temperature changes under nitrogen environment, at 20°C/min, throughout a range from 30°C to 900°C.

The DRP-II thermal conductivity tester was used to measure the thermal conductivity of composite. A sample was cut into a cylinder with a 50 mm radius (R) and 10 mm thickness (h), then a YBF-2 thermal conductivity meter was used for measurement. The thermal conductivity is described according to Eq. (1).

$$\lambda = -mc\frac{2h_p + R_p}{2h_p + 2R_p} \cdot \frac{1}{\pi R^2} \cdot \frac{h}{T_1 - T_2} \cdot \frac{dT}{dt}|T = T_2 \quad (1)$$

where, λ is the thermal conductivity of the sample, $W \cdot m^{-1} \cdot K^{-1}$; m is the mass of the lower copper plate, gm; c is the specific heat capacity of the copper block, R_p and h_p are the radius and thickness of the lower copper plate, mm; R is the radius, mm; h is the height, mm; $T_1 - T_2$ is the temperature difference between the upper and lower copper plates; $\frac{dT}{dt}|T = T_2$ is the rate of cooling of the copper plate exposed to the air.

The FTT0077 oxygen index meter was used to measure the LOI of the composite at room temperature in accordance with the Chinese National Standards GB/T 2406.2-2009, and the samples were customized at 80 mm × 10 mm × 10 mm.

The TGA-IR spectra of GCW and GCPW1 composites were examined utilizing a thermogravimetric infrared spectrometer (Nicolet Instrument Corp., Madison, WI, USA) at a temperature range of 30°C–600°C and a heating rate of 10°C/min in a nitrogen environment.

2.3.6 Horizontal Combustion, UL-94 Vertical Combustion Tests

A butane torch was used as the flame source for the horizontal combustion test, fixed at a distance of 3 mm between the muzzle and the composite material. Vertical combustion tests were conducted using a CFZ-2 instrument in accordance with the ANSI/UL 94-2010 standard. Sixparallel tests were performed for each experimental group to obtain the average UL-94 grade.

2.3.7 Cone Calorimeter Test

Powdered and dried samples were tested using a cone calorimeter instrument, FTT0007, in accrodance with the ASTM E1354 standard. The radiation intensity was 25 kW/m^2.

2.3.8 Biodegradable Performance Testing

According to pertinent literature [32], GCPW1 was encased in polyethylene plastic mesh and thereafter positioned in a polyethylene basin. The sample was situated 150–200 mm beneath the surface soil of the basin. Soil samples were collected regularly every 3 to 5 days. All residual debris from the sample's surface was removed and subsequently dried for mass measurement. After a 15-day interval, the degradation residue was subjected to Fourier Transform Infrared (FTIR) analysis.

3 Results and Discussion

Citric acid, GC, and GCP showed C=O stretching vibrations at 1730 cm^{-1} (Fig. 1a), which are attributed to the -COOH group, whereas this peak was absent in glucose [33]. The peak detected in the GC curve at 1180 cm^{-1} is attributed to the C-O-C group of carbonyl or ester groups [34]. On the contrary, the magnified image of citric acid at 1180 cm^{-1} shows no discernible characteristic peak (marked by a red square), suggesting an esterification reaction between citric acid and glucose. The peak at 1200 ppm is attributed to the ester group [35,36]; compared to the GC curve, the peak at 1200 cm^{-1} in GCP shifted, and the addition of PVA changed the chemical environment of the GC system, suggesting that GC and PVA underwent an esterification reaction.

In contast to citric acid, GC and GCP resins showed a C1 peak at around 172 ppm, and a significant decrease in the C2 peak near 174 ppm (Fig. 1b), due to the formation of carbonyl groups [37]. The peak of GCP at 147 ppm is weaker than that of GC, indicating that the addition of PVA affects the esterification reaction of GCP and CP.

In contrast to the crystallinity of glucose and citric acid (88.37% and 86.17%, respectively), the spectra of GC and GCP exhibit low intensity (Fig. 1c), broad diffraction peaks, and high amorphous scattering halos, which are typical characteristics of semi crystalline polymers with low crystallinity [38]. This suggests the esterification and condensation reaction between citric acid and glucose reduces the crystallinity of glucose. Meanwhile, the crystallinity of GCP (15.04%) was lower than that of GC (21.75%), indicating that a portion of PVA intereacted with the GC system.

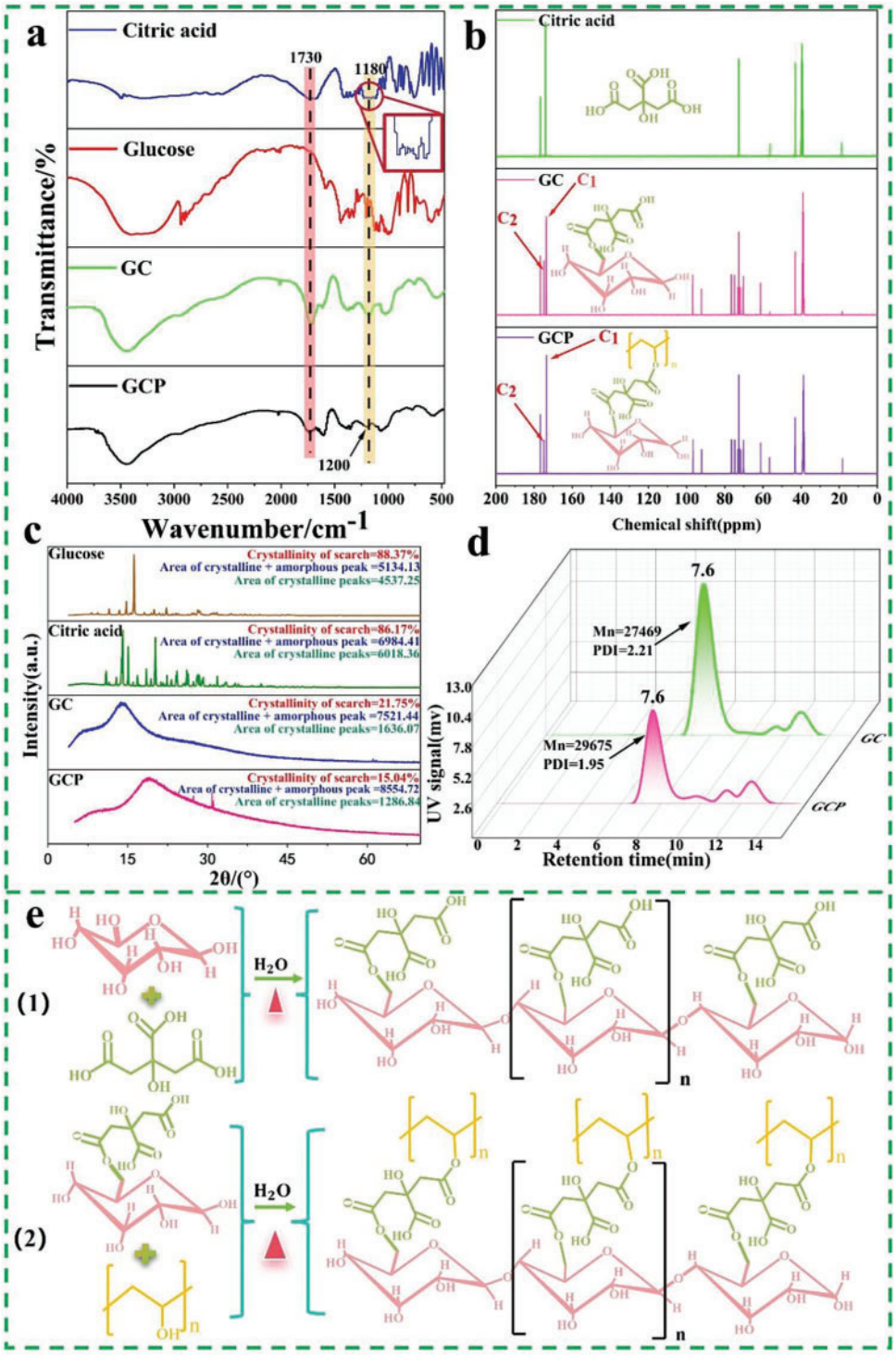

Figure 1: FTIR spectra of Citric acid (C), Glucose (G), GC, and GCP (a), C^{13}—Nuclear Magnetic Resonance (NMR) spectra of C, GC, and GCP (b), XRD spectra of C, G, GC, and GCP (c), GPC chromatograms of G, GC, and GCP (d), main chemical reactions in GCP resin synthesis (e)

The Gel permeation chromatography (GPC) chromatograms of GC and GCP are shown in Fig. 1d. The Mn of GCP (40,257 g/mol) is higher than that of GC (29,675 g/mol), while its retention time (1.95 min) is

shorter than that of GC (2.21 min). This signifies an interaction between GC resin and PVA. In addition, the Mw of GCP (78,314 g/mol) is greater than that of GC (65,554 g/mol), indicating that PVA and GC resin have formed a large number of hydrogen bonds, with longer chain segments [39].

The specific reaction for the formation of GCP resin is as follows: glucose undergoes esterification reaction with the hydroxyl groups of citric acid to remove water molecules at a temperature of 80°C, resulting in the formation of GC resin as shown in Fig. 1e(1). Then, the hydroxyl groups of GC resin undergo an esterification reaction or form hydrogen bonds with the hydroxyl groups of PVA to further produce GCP resin, as shown in Fig. 1e(2).

Compared to the deconvolution spectrum of C1s peak of citric acid (Fig. 2c), the deconvolution spectrum of the C1s peaks for GC, GCP, and GCP1 (Fig. 2f,i, and l) showed a peak at 286.9 eV, which is attributed to the C-O-C functional group [40–42], signifying an esterification reaction between glucose and citric acid. Meanwhile, in comparison to the X-ray photoelectron spectroscopy (XPS) spectrum of GCP (Fig. 2g), the XPS spectrum of GCP1 showed a B1S peak at about 173.9 eV (Fig. 2j), and a peak at 533.0 eV was observed in the deconvolution spectrum of the O1s peak of GCP1 (Fig. 2k), which is attributed to the O-B bond [43], indicating the successful incorporation of boric acid into the GCP resin.

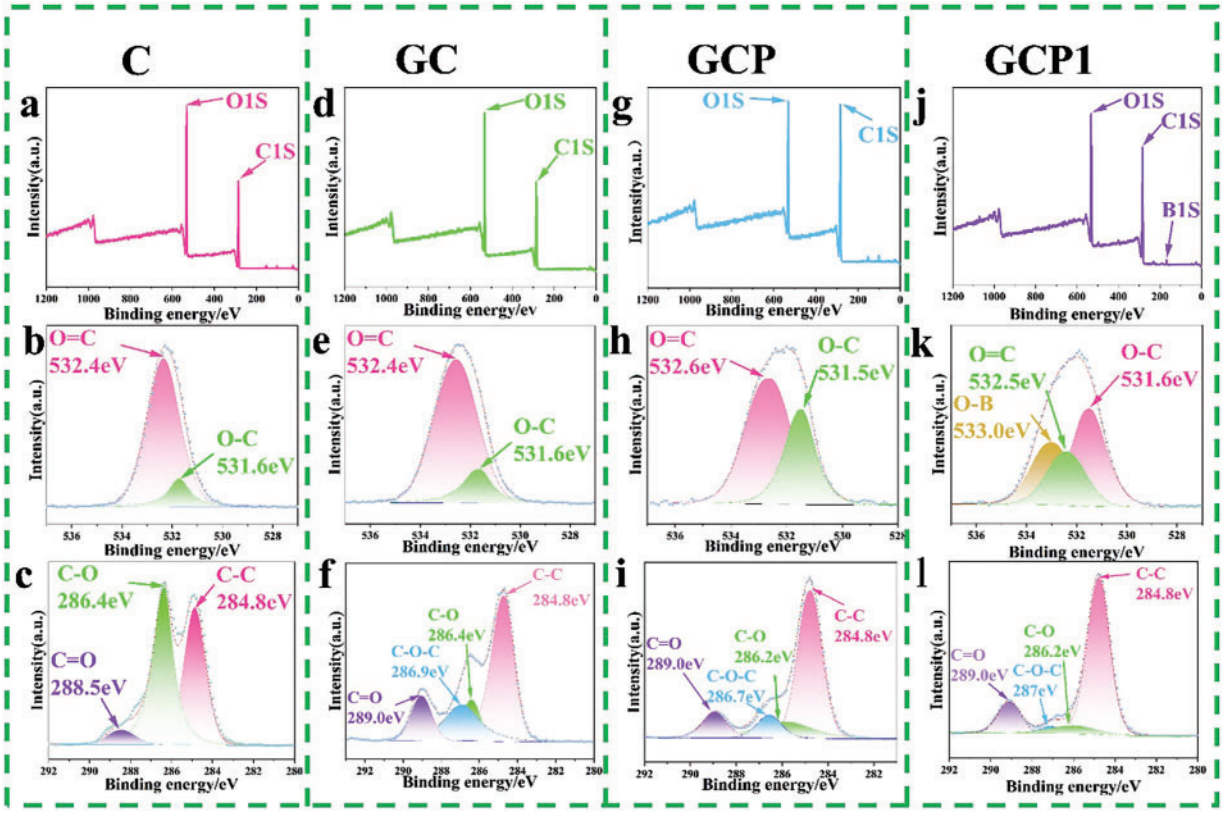

Figure 2: (a) XPS spectrum of citric acid, (b) deconvolution spectrum of O1s peak of citric acid, (c) deconvolution spectrum of C1 s peak of citric acid, (d) XPS spectrum of GC resin, (e) deconvolution spectrum of O1s peak of GC resin, (f) deconvolution spectrum of C1s peak of GC resin, (g) XPS spectrum of GCP resin, (h) deconvolution spectrum of O1s peak of GCP resin, (i) deconvolution spectrum of C1s peak of GCP resin, (j) XPS spectrum of GCP1 resin, (k) deconvolution spectrum of O1s peak of GCP1 resin, (l) deconvolution spectrum of C1s peak of GCP1 resin deconvolutional spectrum of peaks

The appearance and Scanning Electron Microscope (SEM) of various glucose resin-based composites are illustrated in Fig. 3a and b. From Fig. 3a, the surfaces of all samples are relatively flat, with the presence of some pores. In addition, the surface pores of GCPW1 are fewer than those of GCPW2, and the surface of GCPW1 is smoother, suggesting that the blending effect of 2 g boric acid with GCP resin and WSP is better than that of 4 g boric acid. Furthermore, Fig. 3b shows the microstructure of different glucose resin-based composites. At a magnification of 250 μm, the surface roughness of GCPW (Fig. 3b-5) and GCW (Fig. 3b-1) is similar. However, upon magnification to 10 and 5 μm, the smoothness of the surface of GCPW (Fig. 3b-8) surpasses that of GCW (Fig. 3b-4), concurrently revealing significant WSP aggregation appeared in GCW (Fig. 3b-2). It is worth noting that the appearance of GCPW1 (Fig. 3b-9) is flatter and denser than that of GCW (Fig. 3b-1), GCPW (Fig. 3b-5), and GCPW2 (Fig. 3b-13). Moreover, as shown in Fig. 3b-15, there are large pores and particle aggregation inside GCPW2. The results indicate that adding an appropriate amount of boric acid can promote a denser internal structure of the composite, with almost no large pores inside the GCPW1 composite. However, as the amount of boric acid increases, particle aggregation will occur, resulting in the formation of larger pores during the curing process.

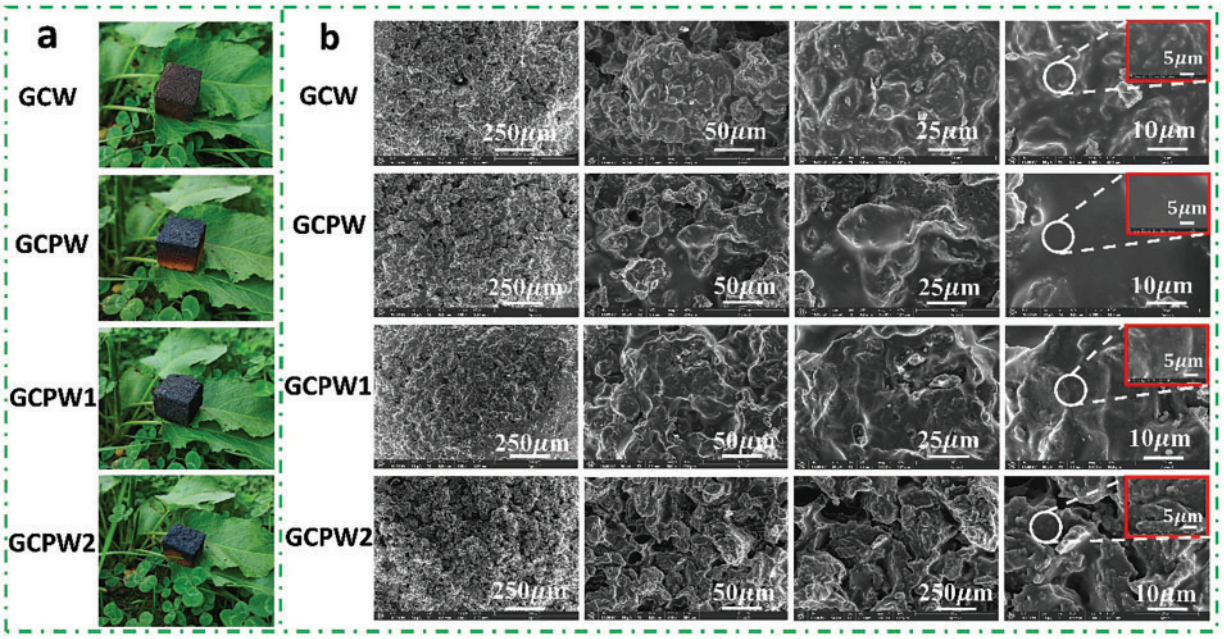

Figure 3: The appearance (a) and SEM image (b) of different glucose resin-based composites

Fig. 4a illustrates the compressive strength of glucose resin-based composites, demonstrating that the compressive strength of GCPW composites surpasses that of GCW, recorded at 6.35 MPa. The hydrogen bonding between PVA and GC resin, as evidenced by FTIR and 13C-NMR results, facilitates the formation of a cross-linked network structure, culminating in a denser internal composite structure, as illustrated in the SEM result (Fig. 3b). The compressive strength of GCPW1 (9.15 MPa) exceeds that of GCPW (8.17 MPa) and GCPW2 (7.66 MPa).

The SEM analysis indicates that the incorporation of an appropriate quantity of boric acid enhances the compatibility between WSP and GCP resin. Nevertheless, an increase in the quantity of added boric acid leads to particle agglomeration, which diminishes the mechanical characteristics of the composite, as evidenced by the SEM data.

Fig. 4c shows the apparent density of different glucose resin-based composites. The apparent density of GCW is 0.87 g/cm^3. Upon the addiiton of PVA, the apparent density of the GCPW increases to 1.04 g/cm^3, further indicating that PVA forms a dense network structure with GC resin through esterification crosslinking and hydrogen bonding. The apparent density of the GCPW1 composite reached 1.3 g/cm^3 after boric addition, indicating that an appropriate amount of boric acid was well dispersed in the GCP resin in alongside WSP. However, as the amount of boric acid rose, the apparent density of the GCPW2 composite was lower than that of GCPW1 composite, indicating that an excess of boric acid promotes particle aggregation in the GCP resin, hence compromising the density of the composite. Fig. 4d shows the pulverization ratios of different glucose resin-based composites. All composites exhibit lower pulverization ratios, all <1%, demonstrating good wear resistance [44]. Moreover, the pulverization ratio of GCPW1 (0.1%) is lower than that of GCW (0.6%), indicating that the addition of PVA improves the toughness and strength of the composites.

Fig. 4e and f illustrates the water absorption and expansion rates of different glucose resin-based polymers. GCW fractures and expands after being submerged in water for 24 h. In comparison to GCW, the incorporation of PVA in GCPW increased its hydroxyl content, primarily facilitating hydrogen bonding with polar water molecules, hence augmenting the hydrophilicity of cellulose and hemicellulose in WSP [45]. Boric acid interacts with the GCP resin and enhances the stability of the internal network structure of GCPW1 due to its unique tetrahedral structure, further improving its water resistance. Fig. 5g shows the water contact angles of different composites. The water contact angle of GCW (109.02°) is lower than that of GCPW (124.80°), indicating that the interaction between PVA and GC resin enhances the hydrophobicity of the GCPW surface. In addition, due to the good compatibility between an appropriate amount of boric acid and the GCP matrix along with WSP particles, the composite structure of GCPW1 is denser (as shown by SEM test results), resulting in a higher water contact angle (136.15°) for GCPW1 compared to GCPW.

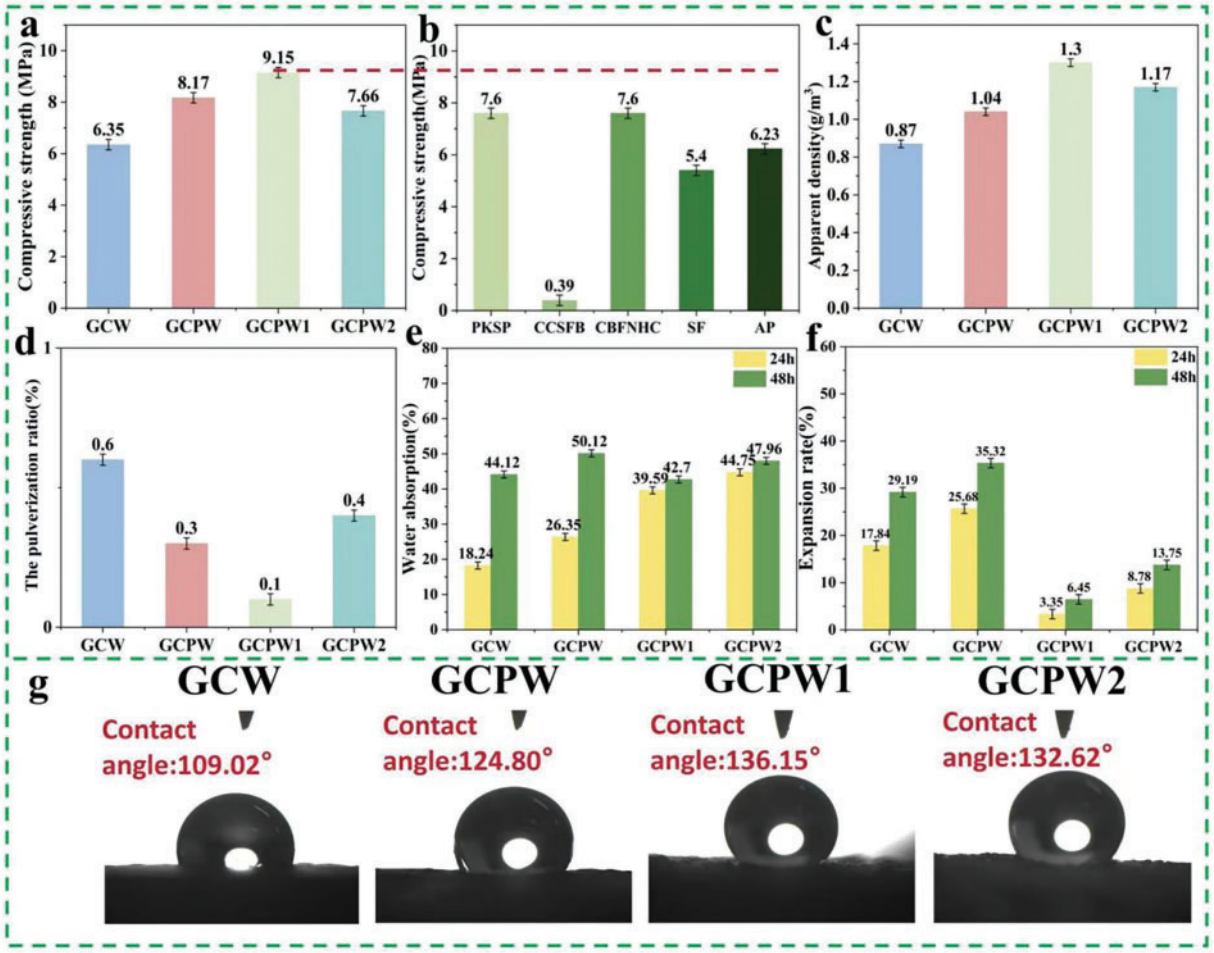

Figure 4: The compressive strength of various glucose resin-based composites (a), the reported compressive strength of composites from literatures [46–50] (b), apparent density (c), pulverization ratio (d), water absorption rate (e), water absorption expansion rate (f), water contact angle (g) of various glucose resin-based composites

All samples exhibit a peak around 80°C, indicating that the mass loss occurs rapidly, depending on the volatilization of volatile substances present in the composite sample. According to Fig. 5a and b, in conjuction with Table 2, all laboratory prepared composites have two main weight reduction stages. The quality loss of GCPW1 in the first stage (15%) is higher than that of GCW (21.5%) and GCPW (17.38%), and lower than that of GCPW2 (8.62%), indicating that the quality loss is attributed to the partial chemical bond damage in the GCP resin matrix within the temperature range of 200°C–250°C [51]. Furthermore, the addition of boric acid does improve the thermal stability of the GCPW composite. The mass loss of GCPW2 in the second stage (52.12%) is higher than that of GCPW1 (39.17%), and at 800°C, the remaining mass of GCPW1 (34.08%) is higher than that of GCPW2 (22.51%), indicating that the thermal stability of GCPW1 is higher than that of GCPW2 when the temperature is higher than 300°C. Despite GCPW2 containing a higher boric acid concentration than GCPW1, SEM analysis shows that the blended particles in GCPW2 agglomerate, preventing uniform dispersion in GCP resin. This leads to poor compatibility between the two, adversely affecting the thermal stability of the composite.

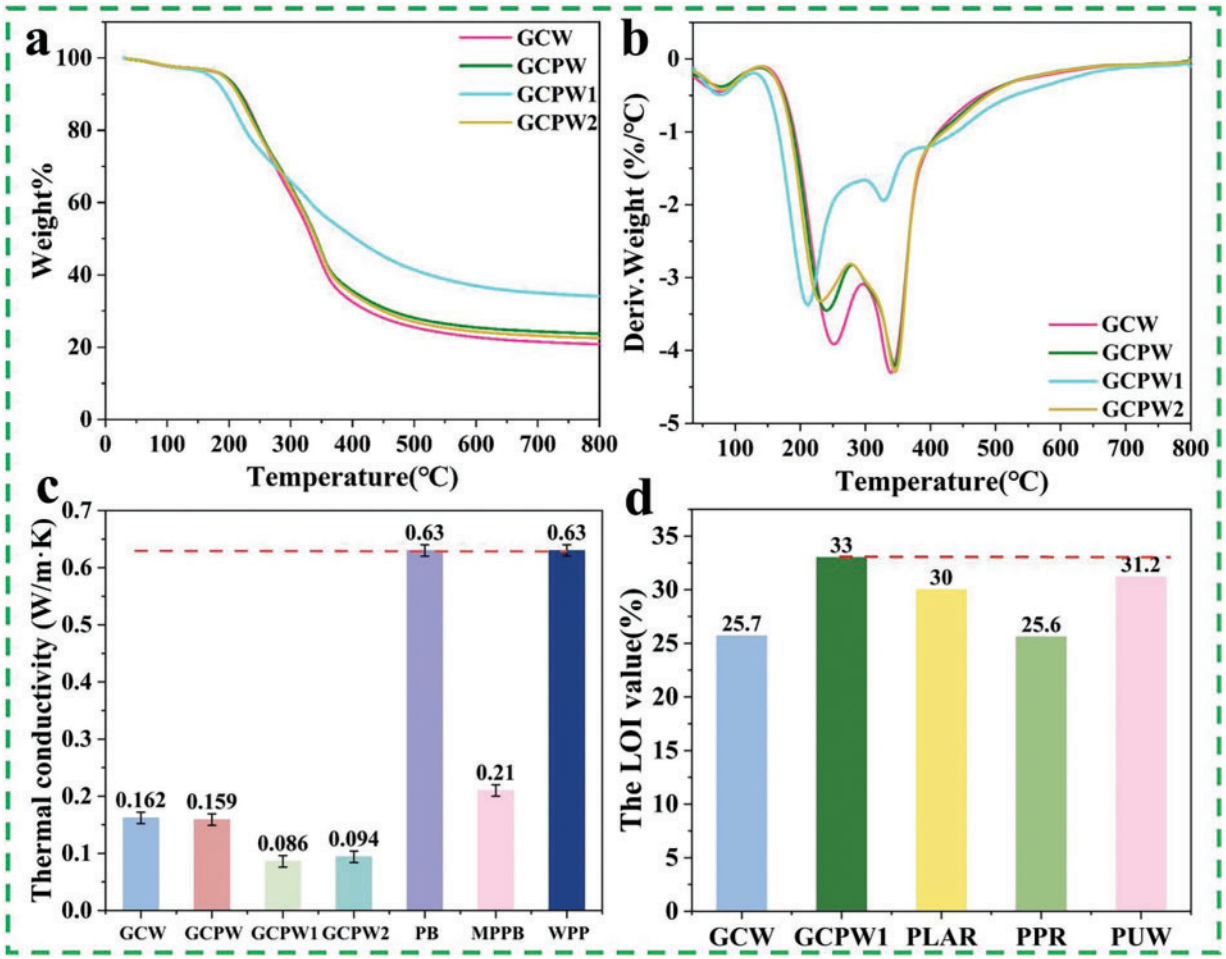

Figure 5: Thermogravimetry (TG) curves (a) and Derivative Thermogravimetry (DTG) curves (b) of various glucose resin-based composites, and thermal conductivity (c) and limit oxygen index (d) of various glucose resin-based composites and various reported composites

Table 2: Thermogravimetric analysis data of various glucose resin-based composites

Sample	Tpeak/°C		Weight loss/%		Residual mass at 800°C/%
	Step I	Step II	Step I	Step II	
GCW	252.7	339.1	21.50	52.20	20.82
GCPW	240.7	345.0	17.38	51.67	23.74
GCPW1	211.4	328.1	15.00	39.17	34.08
GCPW2	209.5	345.5	8.62	52.12	22.51

Fig. 5c illustrates that the thermal conductivity of GCPW (0.159 W/m·K) is inferior to that of GCW (0.162 W/m·K), suggesting that the incorporation of PVA enhances the thermal insulation properties of the composite. Indeed, the addition of PVA improves the crosslinking properties of GC resin, leading to an increase in the density of the composite (shown in Fig. 4c), which further enhances the thermal insulation performance of the composite.

The thermal conductivity of GCPW1 (0.086 W/m·K) is inferior to that of GCPW, suggesting that the use of boric acid enhances the thermal insulation of the composite. Due to the higher compatibility between WSP and GCP resin in GCPW1 compared to GCPW2, the thermal insulation ability of GCPW1 is better than that of GCPW2. Meanwhile, the thermal conductivity of GCPW1 is lower than phenolic-boron nitride composite (PB,0.63 W/m·K) [52], melamine- polyphosphate-boron nitride composite (MPPN, 0.21 W/m·K) [53] and wool reinforced polypropylene composite (WPP, 0.63 W/m·K) [54].

Fig. 5d illustrates that the LOI value of GCW is 25.7%, which is below 27%, signifying that it is a combustible material [55]. Relevant literature [56] indicates that a material is categorized as flame retardant if itsLOI value exceeds 27%. The LOI value of GCPW1 (33%) is significantly exceeds 27%, affirming its classification as a flame retardant composite. This suggests that the incorporation of boric acid enhances flame retardant efficacy; at elevated temperatures, borate liquefies to create a boron-containing glass coating, which obstructs oxygen ingress and heat transfer [57]. Significantly, the LOI value of GCPW1 surpasses that of many documented construction materials, including polylactic acid resin-based composite (PLAR, 30.0%) [58], polypropylene resin-based composite (PPR, 25.6%) [59], and polyurethane/wood fiber composite (PUW, 31.2%) [60].

Fig. 6 depicts the analysis of gaseous emissions from GCW and GCPW1 composites using TGA-FTIR at different temperatures. The primary volatile compounds found in GCW and GCPW1 are H_2O (713 cm^{-1}) [61], CO_2 (2360 cm^{-1}) [62], and CO (2182 cm^{-1}), with these absorption peaks arising from the high-temperature decomposition of the complex. Furthermore, B-O (1756 cm^{-1}) [63] represents the absorption peak associated with the disintegration of boron-containing chain segments in the GCPW1 composite. The infrared spectra of CO_2 (2360 cm^{-1}), CO (2182 cm^{-1}), and B-O (1756 cm^{-1}), as decomposed by GCW and GCPW1, are presented in Fig. 6c. The peak intensity of gaseous products in GCPW1 is lower to that in GCW, suggesting that the incorporation of boron-containing fragments may enhance the carbonization capacity of GCPW1 composites, suppress the cis elimination reaction of the matrix, and reduce hydrocarbon production [64].

No flame dripping phenomenon was observed during the combustion process of GCW, GCPW, GCPW1, and GCPW2 (Fig. 7a). GCPW showed slight cracks (indicated by the red circle) after 120 s of combustion, possibly due to the flammability of unreacted PVA [65,66]. Nonetheless, GCPW1 and GCPW2 exhibited no fissures after 120 s of combustion, demonstrating that the use of boric acid enhanced the flame retardancy of GCPW composites. It is evident from Fig. 7b that both GCW and GCPW1 exhibit secondary combustion without dripping and possess of self-extinguishing capabilities, thus achieving the UL-94 V-0 flame retardant classification and demonstrating superior flame retardant properties. Conversely, the GCW emitted a significant volume of smoke after being extinguished, whereas the GCPW1 sample produced smoke following extinguishment. This results from the creation of a glassy coating on the polymer surface by boric acid, which suppresses smoke production [67].

The peak of HRR (pHRR) of GCW is 388.57 kW/m^2 (Fig. 8a), whereas the pHRR of GCPW1 (176.91 kW/m^2) is 45.53% lower than that of GCW. Meanwhile, Fig. 8b shows that the THR of GCW (40.71MJ/m^2) is much higher than that of GCPW1 (31.91 MJ/m^2). The FIGRA of GCW (6.77 $kW/m^2/s$) is higher than that of GCPW1 (2.62 $kW/m^2/s$) (Table 3), indicating that GCPW1 is more likely to reduce the probability of fire occurrence compared to GCW. Moreover, the time to ignition (TTI) of GCPW1(27s) is higher than that of GCW (15s). At the same time, the Average effective heat of combustion (AEHC) (27.02 MJ/kg) of GCW was higher than that of GCPW1 (22.30 MJ/kg). The TSP (Fig. 8c) and pSPR (Fig. 8d) of GCPW1 are 0.00015 m^2/s and 0.00015 m, respectively, which is 95.5% and 98.5% lower than those of GCW (0.32 m^2/s, 0.01 m^2), respectively. This further indicates that the addition of boric acid effectively blocks smoke during combustion. In the structure of GCPW1 composite, boric acid and WSP are uniformly dispersed

in GCP resin. During combustion, the borate melts and forms a glass covering layer on the surface of the composite, which acts as an oxygen barrier. Boric acid can catalyze the dehydration of WSP at relatively low temperatures (about 100°C–300°C) [68] and react with cellulose in WSP to form borate with excellent self extinguishing properties [69]. The process is shown in Fig. 8e. Besides, the appearance of GCW and GCPW1 after cone calorimeter testing is shown in Fig. 8f. The flame retardant index (FRI) serves as an important indicator for assessing the flame retardant efficacy of composites. The ranking of flame-retardant polymer composites is categorized as poor (FRI < 1), good (1 ≤ FRI < 10), or excellent (FRI ≥ 10) [70]. Table 3 reveals that the FRI of the GCPW1 is 5.04, which is higher than that of GCW (0.91) and GCPW, thereby affirming its good ranking and indicating that the addition of boric acid enhances the flame retardancy of the composite. Furthermore, as the boric acid content increases, the flame retardancy also increasesThe FRI of GCPW2 surpasses that of GCPW1 for this reason.

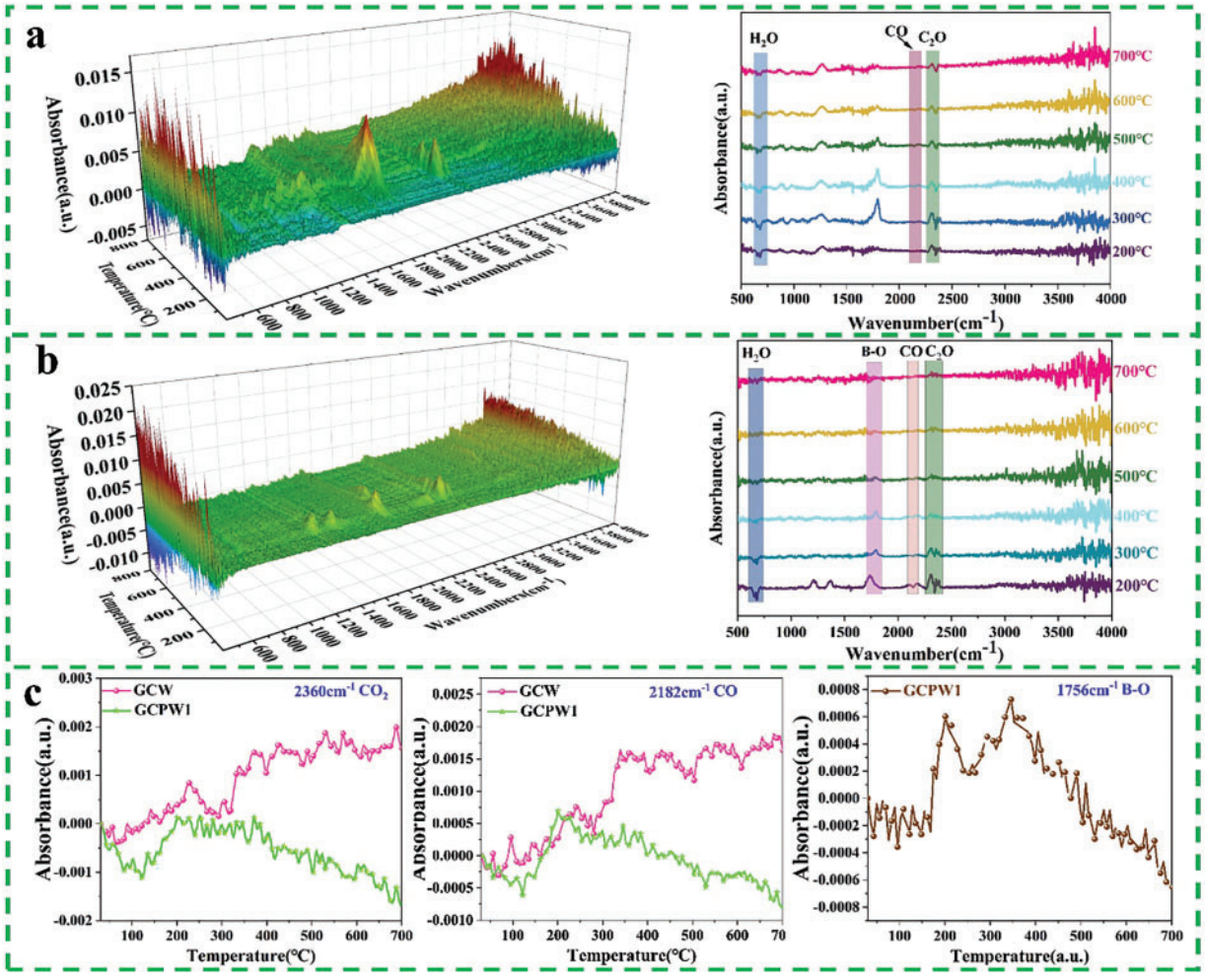

Figure 6: Three-dimensional TGA-FTIR images of GCW (a) and GCPW1 (b), as well as the infrared spectra of gas decomposition products at different temperatures, the main gas volatiles of GCW and GCPW1 (c)

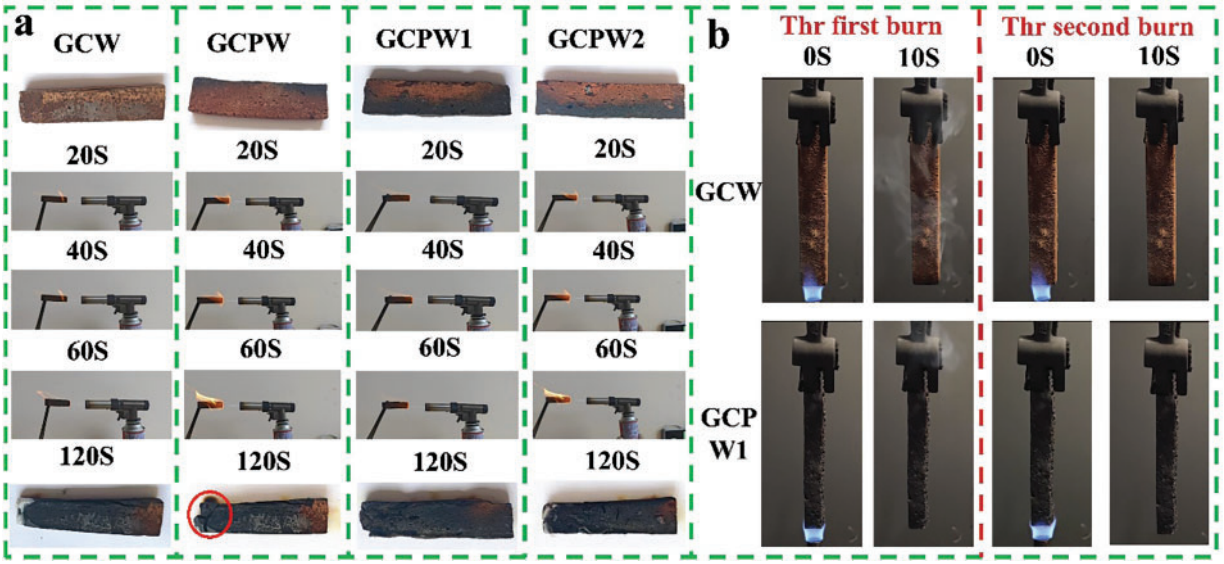

Figure 7: Horizontal combustion test of various glucose resin-based composites (a), UL-94 vertical combustion level test of GCW and GCPW1 composites (b)

The GCW composite exhibits minimal residue post-combustion, however the GCPW1 composite can generate a block-shaped carbon layer after combustion, demonstrating reduced mass loss and effective flame retardancy.

As shown in Figs. 9a, a small amount of mass loss has been detected after a 5-day burial test. The weight loss of GCPW composite was 1.6% higher than GCPW1, indicating that boric acid affected the natural degradation ability of GCPW composites, albeit to a little extent.. Boric acid, while demonstrating low acute toxicity to people and animals, necessitates administration in regulated amounts and adherence to proper disposal protocols. The mass loss GCPW1 was 3.4% during a period of 15 days. SEM test results show that the compactness of the internal structure of GCPW1 is higher than that of GCPW2, which exhibits porosity and particle aggregation. Compared with Fig. 1a (FTIR before degradation), the most significant change is the appearance of two new peaks, which correspond to hydroxyl groups at 3340 cm^{-1} and carboxyl groups at 2930 cm^{-1} (Fig. 9b), signifying localized disintegration of the network structure established by the resin and cellulose in WSP. The peak at 2930 cm^{-1} corresponds to the breaking of C-H bonds in saturated carbon, associated with the vibrations of fatty acids, signifying the synthesis of fatty acid molecules following degradation [71]. The above results demonstrate that the GCPW1 composite has a low degradation rate, suggesting it may retain functionality longer in applications requiring temporary durability, such as construction and building materials.

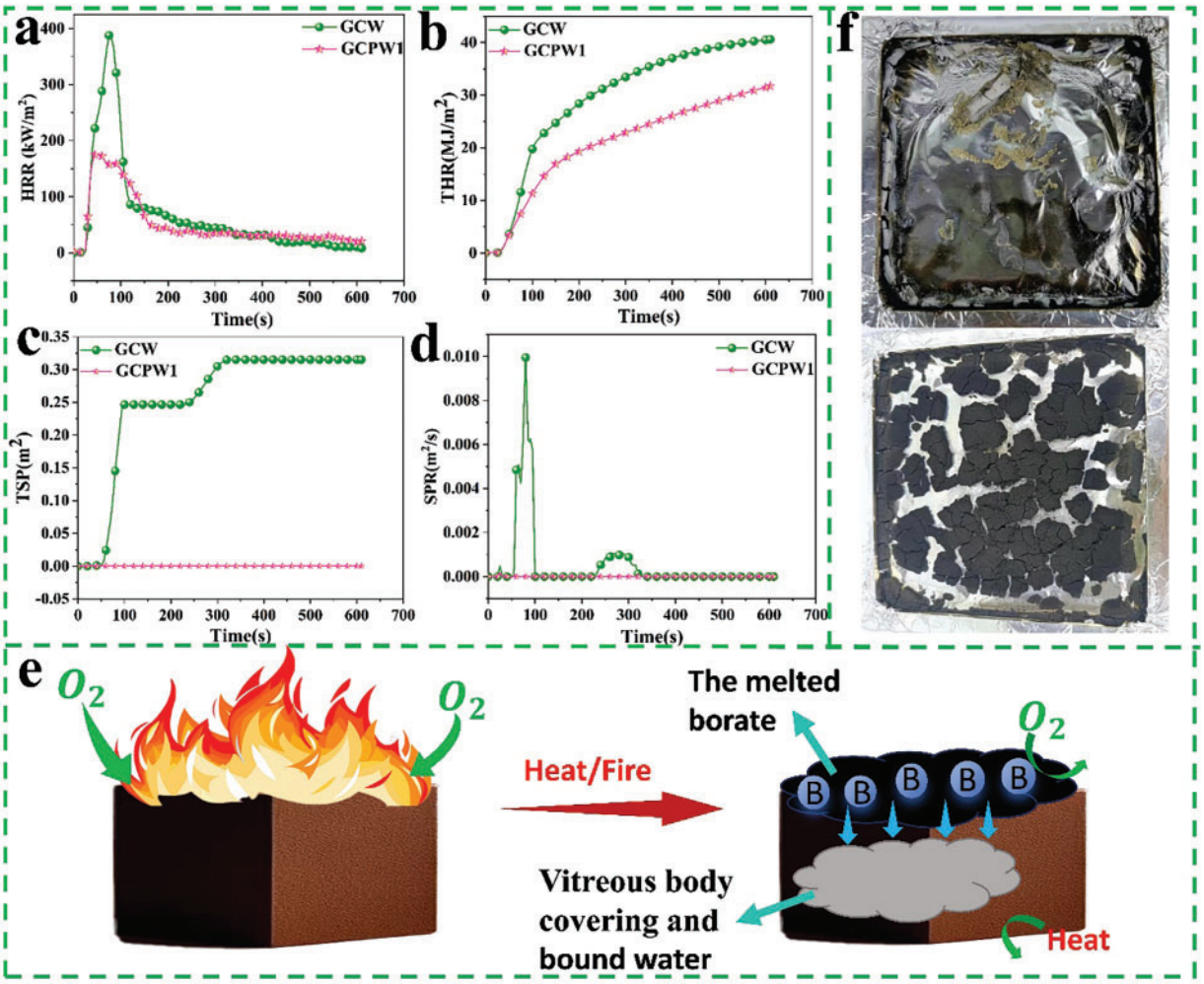

Figure 8: HRR (a), THR (b), TSP (c), and SPR (d) of GCW and GCPW1 composites, flame retardant mechanism of GCPW1 (e), GCW and GCPW1 composites after cone calorimeter testing (f)

Table 3: Cone calorimeter test data for GCW and GCPW1

Sample	TTI (s)	pHRR (kW/m²)	THR (MJ/m²)	pSPR (m²/s)	TSP (m²)	Residue (%)	FIGRA (kW/m²/s)	AEHC (MJ/kg)	FRI
GCW	15	388.57	40.71	0.01	0.32	3.4	6.77	27.02	0.91
GCPW	17	309.68	38.32	0.02	0.26	4.7	5.25	26.86	1.51
GCPW1	27	176.91	31.91	0.00015	0.00015	19.45	2.62	22.30	5.04
GCPW2	36	152.34	26.77	0.00006	0.00006	26.25	3.96	29.07	9.31

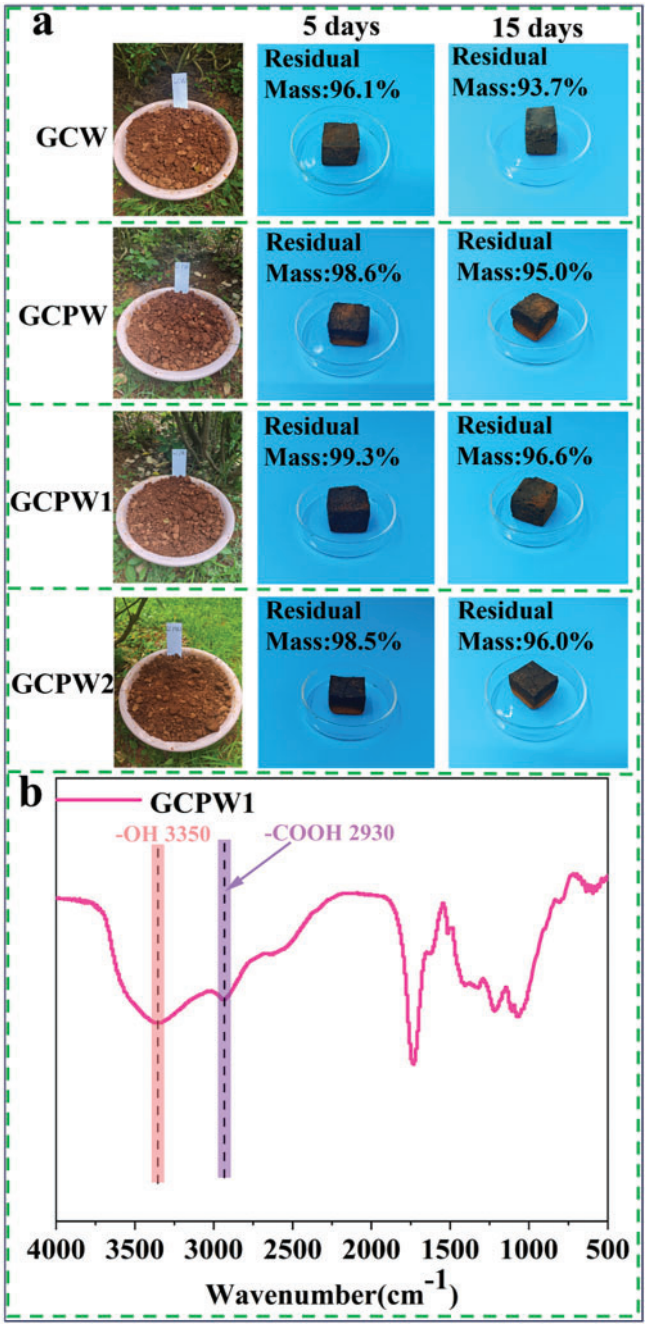

Figure 9: (a) Appearance and residual of composites after 5- and 15-days burial, (b) FTIR spectra of GCPW1 after degradation

4 Conclusions

The hypothesis of the study has been confirmed and proved. A novel building material, termed GCPW, has been developed. A GC resin matrix was specifically formulated using glucose and citric acid derived from biomass as the primary raw materials, followed by the addition of PVA to enhance the toughness of the GC resin. Indeed, the synergistic interaction between WSP and boric acid imparts improved flame retardant properties to GCPW. The maximum LOI value reaches 33% and the FRI has reached a good ranking for flame

retardant materials, satisfying the UL-94 V-0 flame retardant testing requirement. Furthermore, GCPW exhibits elevated compressive strength and a minimal pulverization rate. Significantly, GCPW demonstrates exceptional thermal stability and insulating characteristics. However, the glucose-citric acid composite manufacturing process remains at the laboratory scale and may necessitate optimization for enhanced energy and time efficiency in industrial applications.

Acknowledgement: Not applicable.

Funding Statement: This work was supported by the Natural Science Foundation of China (32460363), Yunnan Province Agricultural Joint Key Foundation (No. 202401BD070001-029), Yunnan Agricultural Joint General Foundation (202101BD070001-105), and, as well as the Yunnan Provincial Youth Top Talent Project (Grant No. YNWR-QNBJ-2020-166), the Foreign Expert Workstation (202305AF150006), the 111 Project (D21027).

Author Contributions: The authors confirm contribution to the paper as follows: Conceptualization, Longjiang Liu and Xiaojian Zhou; methodology, Seng Hua Lee and Wei Chen Lum; software, Wenqing Yang; validation, Jun Zhang, Seng Hua Lee and Wei Chen Lum; formal analysis, Seng Hua Lee; investigation, Zhenzhou Wang and Rui Luo; data curation, Wenqing Yang; writing—original draft preparation, Zhenzhou Wang; writing—review and editing, Jun Zhang, Seng Hua Lee and Xiaojian Zhou; visualization, Longjiang Liu; supervision, Jun Zhang; project administration, Jun Zhang; funding acquisition, Jun Zhang. All authors reviewed the results and approved the final version of the manuscript.

Availability of Data and Materials: Data available on request from the authors.

Ethics Approval: Not applicable.

Conflicts of Interest: The authors declare no conflicts of interest to report regarding the present study.

References

1. Ngo T. Development of sustainable flame-retardant materials. Green Mater. 2020;8(3):101–22. doi:10.1680/jgrma.19.00060.
2. Tian H, Guo G, Fu X, Yao Y, Yuan L, Xiang A. Fabrication, properties and applications of soy-protein-based materials: a review. Int J Biol Macromol. 2018;120(1):475–90. doi:10.1016/j.ijbiomac.2018.08.110.
3. Zheng Z, Chen C, Huang Y, Ou R, Hu C, Wang X, et al. Developing a unilaterally surface-densified wood composite with excellent performance through surface impregnation of furfuryl alcohol resin. ACS Appl Polym Mater. 2022;4(8):5308–18. doi:10.1021/acsapm.2c00279.
4. Yang K, Zhang Z, Liu Y, Li S, Chen D, Li Z. Biomass-based porous composites with heat transfer characteristics: preparation, performance and evaluation—a review. J Porous Mater. 2022;29(6):1667–87. doi:10.1007/s10934-022-01296-0.
5. Deng J, Zhu E-Q, Xu G-F, Naik N, Murugadoss V, Ma M-G, et al. Overview of renewable polysaccharide-based composites for biodegradable food packaging applications. Green Chem. 2022;24(2):480–92. doi:10.1039/D1GC03898B.
6. Hejna A. Renewable, degradable, and recyclable polymer composites. Polymers. 2023;15(7):1769. doi:10.3390/polym15071769.
7. Lee SH, Md Tahir P, Lum WC, Tan LP, Bawon P, Park BD, et al. A review on citric acid as green modifying agent and binder for wood. Polymers. 2020;12(8):1692. doi:10.3390/polym12081692.
8. Widyorini R, Nugraha PA, Rahman MZA, Prayitno TA. Bonding ability of a new adhesive composed of citric acid-sucrose for particleboard. BioResources. 2016;11(2):4526–35. doi:10.15376/biores.11.2.4526-4535.
9. Li C, Lei H, Wu Z, Xi X, Du G, Pizzi A. Fully biobased adhesive from glucose and citric acid for plywood with high performance. ACS Appl Mater Interfaces. 2022;14(20):23859–67. doi:10.1021/acsami.2c02859.

10. Choi HW. From the photosynthesis to hormone biosynthesis in plants. Plant Pathol J. 2024;40(2):99–105. doi:10.5423/PPJ.RW.01.2024.0006.
11. Siddiqui H, Sami F, Glucose Hayat S. Sweet or bitter effects in plants—a review on current and future perspective. Carbohydr Res. 2020;487:107884. doi:10.1016/j.carres.2019.107884.
12. Zhu X, Shen S, Tang Z, Yang J. Ti^{3+}-doped TiO_2@C nanorods with enhanced photocatalytic performance under visible light. Compos Interfaces. 2020;27(3):263–75. doi:10.1080/09276440.2019.1623608.
13. Poletti Papi MA, Caetano FR, Bergamini MF, Marcolino-Junior LH. Facile synthesis of a silver nanoparticles/polypyrrole nanocomposite for non-enzymatic glucose determination. Mater Sci Eng C. 2017;75:88–94. doi:10.1016/j.msec.2017.02.026.
14. Abdelaziz SA, Ahmed EM, Sadek M. Synthesis of homologous series of surfactants from renewable resources, structure-properties relationship, surface active performance, evaluation of their antimicrobial and anticancer potentialities. Sci Rep. 2024;14(1):13201. doi:10.1038/s41598-024-62905-3.
15. Mukherjee C, Varghese D, Krishna JS, Boominathan T, Rakeshkumar R, Dineshkumar S, et al. Recent advances in biodegradable polymers—properties, applications and future prospects. Eur Polym J. 2023;192(9):112068. doi:10.1016/j.eurpolymj.2023.112068.
16. Hollenbach R, Bindereif B, Van Der Schaaf US, Ochsenreither K, Syldatk C. Optimization of glycolipid synthesis in hydrophilic deep eutectic solvents. Front Bioeng Biotechnol. 2020;8:382. doi:10.3389/fbioe.2020.00382.
17. Guo W, Xiao Z, Wentzel M, Emmerich L, Xie Y, Militz H. Modification of Scots pine with activated glucose and citric acid: physical and mechanical properties. BioResources. 2019;14(2):3445–58. doi:10.15376/biores.14.2.3445-3458.
18. Lal S, Kumar V, Arora S. Eco-friendly synthesis of biodegradable and high strength ternary blend films of PVA/starch/pectin: mechanical, thermal and biodegradation studies. Polym Polym Compos. 2021;29(9):1505–14. doi:10.1177/0967391120972881.
19. Kuo T-Y, Jhang C-F, Lin C-M, Hsien T-Y, Hsieh H-J. Fabrication and application of coaxial polyvinyl alcohol/chitosan nanofiber membranes. Open Phys. 2017;15(1):1004–14. doi:10.1515/phys-2017-0125.
20. Ge JC, Wu G, Yoon SK, Kim MS, Choi NJ. Study on the preparation and lipophilic properties of polyvinyl alcohol (PVA) nanofiber membranes via green electrospinning. Nanomaterials. 2021;11(10):2514. doi:10.3390/nano11102514.
21. Kumar JA, Sathish S, Prabu D, Renita AA, Saravanan A, Deivayanai VC, et al. Agricultural waste biomass for sustainable bioenergy production: feedstock, characterization and pre-treatment methodologies. Chemosphere. 2023;331(120349):138680. doi:10.1016/j.chemosphere.2023.138680.
22. Abdulwahid MY, Akinwande AA, Kamarou M, Romanovski V, Al-Qasem IA. The production of environmentally friendly building materials out of recycling walnut shell waste: a brief review. Biomass Convers Biorefinery. 2023. doi:10.1007/s13399-023-04760-2.
23. Fordos S, Abid N, Gulzar M, Pasha I, Oz F, Shahid A, et al. Recent development in the application of walnut processing by-products (walnut shell and walnut husk). Biomass Convers Biorefinery. 2023;13(16):14389–411. doi:10.1007/s13399-023-04778-6.
24. Halysh V, Romero-García JM, Vidal AM, Kulik T, Palianytsia B, García M, et al. Apricot seed shells and walnut shells as unconventional sugars and lignin sources. Molecules. 2023;28(3):1455. doi:10.3390/molecules28031455.
25. McNeill DC, Pal AK, Mohanty AK, Misra M. High biomass filled biodegradable plastic in engineering sustainable composites. Composites Part C. 2023;12:100388. doi:10.1016/j.jcomc.2023.100388.
26. Makowska S, Miedzińska K, Kairytė A, Šeputytė-Jucikė J, Strzelec K. Flame retardancy and thermal stability of rigid polyurethane foams filled with walnut shells and mineral fillers. Materials. 2024;17(18):4629. doi:10.3390/ma17184629.
27. Demirhan Y, Yurtseven R, Usta N. The effect of boric acid on flame retardancy of intumescent flame retardant polypropylene composites including nanoclay. J. Thermoplast Compos Mater. 2023;36(3):1187–214. doi:10.1177/08927057211052327.
28. Zhu W, Hao S, Yang M, Cheng B, Zhang J. A synergistic flame retardant of glycosyl cross-linking boron acid and ammonium salt of phytic acid to enhance durable flame retardancy of cotton fabrics. Cellulose. 2020;27(16):9699–710. doi:10.1007/s10570-020-03417-x.

29. Nine MJ, Tran DNH, Tung TT, Kabiri S, Losic D. Graphene-borate as an efficient fire retardant for cellulosic materials with multiple and synergetic modes of action. ACS Appl Mater Interfaces. 2017;9(11):10160–8. doi:10.1021/acsami.7b00572.
30. Bee S-T, Sin LT, Ch'ng BS, Ratnam CT, Rahmat AR. Effect of zinc borate on enhancing flame retardancy of electron beam irradiated alumina trihydrate (ATH)/acrylonitrile butadiene styrene (ABS) composites. Int Polym Process. 2019;34(1):121–32. doi:10.3139/217.3677.
31. Jiang J, Wang W, Lee SH, Lum WC, Essawy H, Du G, et al. Flame retardancy, photostability, and thermal properties of vanillin-epoxidized soybean oil composites reinforced with walnut shell. Ind Crops Prod. 2024;218:118912. doi:10.1016/j.indcrop.2024.118912.
32. Dong Y, Liu B, Lee SH, Lum WC, Ren Y, Zhou X, et al. Fabrication of rigid flame retardant foam using bio-based sucrose-furanic resin for building material applications. Chem Eng J. 2024;495:153614. doi:10.1016/j.cej.2024.153614.
33. Zhou H, Lee SH, Tahir PM, Ashaari Z, Al-Edrus SSO, Ibrahim NA, et al. Physico-mechanical and biological durability of citric acid-bonded rubberwood particleboard. Polymers. 2020;13(1):98. doi:10.3390/polym13010098.
34. Kusumah SS, Umemura K, Yoshioka K, Miyafuji H, Kanayama K. Utilization of sweet sorghum bagasse and citric acid for manufacturing of particleboard I: effects of pre-drying treatment and citric acid content on the board properties. Ind Crops Prod. 2016;84(9):34–42. doi:10.1016/j.indcrop.2016.01.042.
35. Peng J, Zhou C, Chen B, Zhang H, Pan X, Xiong W, et al. Rational design of waterborne biobased epoxy methacrylates using citric acid and epoxy soybean oil for UV-curable coatings. Ind Crops Prod. 2024;209(1–2):117958. doi:10.1016/j.indcrop.2023.117958.
36. Kusumah SS, Jayadi, Wibowo DT, Pramasari DA, Widyaningrum BA, Darmawan T, et al. Investigation of eco-friendly plywood bonded with citric acid-starch based adhesive. IOP Conf Ser Earth Environ Sci. 2020;460(1):012009. doi:10.1088/1755-1315/460/1/012009.
37. Hadinugroho W, Martodihardjo S, Fudholi A, Riyanto S. Esterification of citric acid with locust bean gum. Heliyon. 2019;5(8):e02337. doi:10.1016/j.heliyon.2019.e02337.
38. Zafari R, Fauteux-Lefebvre C. Surface modification investigation of nanocrystalline cellulose with combined functional groups for sulfur dioxide capture. Adsorption. 2023;29:151–61. doi:10.1007/s10450-023-00390-2.
39. Xu X, Xu Y, Deng S, Chen X, Essawy H, Lee SH, et al. Graft copolymer of tannin and polyvinyl alcohol with acrylic acid for the preparation of hydrophobic biodegradable film. Prog Org Coat. 2024;186:108090. doi:10.1016/j.porgcoat.2023.108090.
40. Hoang MT, Pham TD, Pham TT, Nguyen MK, Nu DTT, Nguyen TH, et al. Esterification of sugarcane bagasse by citric acid for Pb^{2+} adsorption: effect of different chemical pretreatment methods. Environ Sci Pollut Res. 2021;28(10):11869–81. doi:10.1007/s11356-020-07623-9.
41. Min X, Han C, Yang L, Zhou C. Enhancing As(V) and As(III) adsorption performance of low alumina fly ash with ferric citrate modification: role of $FeSiO_3$ and monosodium citrate. J Environ Manage. 2021;287:112302. doi:10.1016/j.jenvman.2021.112302.
42. Ding H, Liu D. Preparation and performance of poly(lactic acid)/amidated ammonium citrate intercalated saponite nanocomposites. Polym-Plast Technol Mater. 2020;59(8):809–21. doi:10.1080/25740881.2019.1695270.
43. Tao Y, Huang C, Lai C, Huang C, Yong Q. Biomimetic galactomannan/bentonite/graphene oxide film with superior mechanical and fire retardant properties by borate cross-linking. Carbohydr Polym. 2020;245(55):116508. doi:10.1016/j.carbpol.2020.116508.
44. Oladele IO, Makinde-Isola BA, Adediran AA, Oladejo MO, Owa AF, Olayanju TMA. Mechanical and wear behaviour of pulverised poultry eggshell/sisal fiber hybrid reinforced epoxy composites. Mater Res Express. 2020;7(4):045304. doi:10.1088/2053-1591/ab8585.
45. Czibulya Z, Csík A, Tóth F, Pál P, Csarnovics I, Zelkó R, et al. The effect of the PVA/chitosan/citric acid ratio on the hydrophilicity of electrospun nanofiber meshes. Polymers. 2021;13(20):3557. doi:10.3390/polym13203557.
46. Ezema Ike-Eze IC, Uyor UO, Aigbodion VS, Omah AD, Ude SN, Daniel-Nkpume CC. Tensile and compressive strength of palm kernel shell particle reinforced polyester composites. Mater Res Express. 2019;6(11):115335. doi:10.1088/2053-1591/ab4afa.

47. Ma C, Zhang S, Dong R, Wang M, Jia W, Lu Z. Corn stalk fiber-based biomass brick reinforced by compact organic/inorganic calcification composites. ACS Sustain Chem Eng. 2018;6(2):2086–93. doi:10.1021/acssuschemeng.7b03509.
48. Tang S, Jiang L, Jiang Z, Ma Y, Zhang Y, Su S. Improving the mechanical, degradation properties and biocompatibility of nano-hydroxyapatite/chitosan composite scaffold by the introduction of carboxylated bamboo fiber. Cellulose. 2023;30(3):1585–97. doi:10.1007/s10570-022-05001-x.
49. Zhang J, Liu B, Zhou Y, Essawy H, Zhao C, Wu Z, et al. Gelatinized starch-furanic hybrid as a biodegradable thermosetting resin for fabrication of foams for building materials. Carbohydr Polym. 2022;298(2):120157. doi:10.1016/j.carbpol.2022.120157.
50. Yusri MAHM, Zuhri MYM, Ishak MR, Azman MA. the capabilities of honeycomb core structures made of Kenaf/Polylactic acid composite under compression loading. Polymers. 2023;15(9):2179. doi:10.3390/polym15092179.
51. Tu J-L, Yuan J-J. Thermal decomposition behavior of hydroxytyrosol (HT) in nitrogen atmosphere based on TG-FTIR methods. Molecules. 2018;23(2):404. doi:10.3390/molecules23020404.
52. Samoilov VM, Danilov EA, Kaplan IM, Lebedeva MV, Yashtulov NA. Thermal conductivity of polymer composite material based on phenol-formaldehyde resin and boron nitride. Russ Phys J. 2022;65(1):80–90. doi:10.1007/s11182-022-02609-1.
53. Shi X, Wei B, Gao H. Enhanced flame retardancy of epoxy composites containing melamine polyphosphate-modified boron nitride. J Appl Polym Sci. 2022;139(48):e53215. doi:10.1002/app.53215.
54. Ilangovan M, Navada AP, Guna V, Touchaleaume F, Saulnier B, Grohens Y, et al. Hybrid biocomposites with high thermal and noise insulation from discarded wool, poultry feathers, and their blends. Constr Build Mater. 2022;345:128324. doi:10.1016/j.conbuildmat.2022.128324.
55. Chen B, Gao W, Shen J, Guo S. The multilayered distribution of intumescent flame retardants and its influence on the fire and mechanical properties of polypropylene. Compos Sci Technol. 2014;93:54–60. doi:10.1016/j.compscitech.2013.12.022.
56. Ma Y, Ma P, Ma Y, Xu D, Wang P, Yang R. Synergistic effect of multiwalled carbon nanotubes and an intumescent flame retardant: toward an ideal electromagnetic interference shielding material with excellent flame retardancy. J Appl Polym Sci. 2017;134(31):45088. doi:10.1002/app.45088.
57. Wang Q, Li J, Winandy Jerrold E. Chemical mechanism of fire retardance of boric acid on wood. Wood Sci Technol. 2004;38(5):375–89. doi:10.1007/s00226-004-0246-4.
58. Pei M, Wei K, Zhang D, Qin S. Polylactic acid flame-retardant composite preparation and investigation of flame-retardant characteristics. Polym Eng Sci. 2023;63(3):880–94. doi:10.1002/pen.26251.
59. Pérez N, Qi X-L, Nie S, Acuña P, Chen M-J, Wang D-Y. Flame retardant polypropylene composites with low densities. Materials. 2019;12(1):152. doi:10.3390/ma12010152.
60. Wang X, Wang B, Sun J, Yu L, Yang G, Guo H. Flame-retardant composite derived from polyurethane/wood-fiber. Fire Mater. 2024;48(2):273–85. doi:10.1002/fam.3182.
61. Li Y, Sun L, Wang H, Wang S, Jin X, Lu Z, et al. A novel composite coating containing P/N/B and bio-based compounds for flame retardant modification of polyester/cotton blend fabrics. Colloids Surf Physicochem Eng Asp. 2023;660(10):130826. doi:10.1016/j.colsurfa.2022.130826.
62. Wang J, Zhou H, Wang Z, Bai W, Cao Y, Wei Y. Constructing hierarchical structure based on LDH anchored boron-doped g-C_3N_4 assembled with MnO_2 nanosheets towards reducing toxicants generation and fire hazard of epoxy resin. Compos Part B Eng. 2022;229(6):109453. doi:10.1016/j.compositesb.2021.109453.
63. Rudawska A, Frigione M, Sarcinella A, Brunella V, Di Lorenzo L, Olewnik-Kruszkowska E. Properties and performance of epoxy resin/boron acid composites. Materials. 2092;2024(9):2092. doi:10.3390/ma17092092.
64. Zhao X, Guerrero FR, Llorca J, Wang D-Y. New superefficiently flame-retardant bioplastic poly(lactic acid): flammability, thermal decomposition behavior, and tensile properties. ACS Sustain Chem Eng. 2016;4(1):202–9. doi:10.1021/acssuschemeng.5b00980.
65. Wang X, Li Y, Meng D, Gu X, Sun J, Hu Y, et al. A review on flame-retardant polyvinyl alcohol: additives and technologies. Polym Rev. 2023;63(2):324–64. doi:10.1080/15583724.2022.2076694.

66. Xu W, Zhang Y, Liu J, Xuan Z, Su L, Zhao M. Flame retardant polyvinyl alcohol composite with excellent comprehensive properties prepared using Cu_2O/chitosan and phosphorus-based flame retardants. Iran Polym J. 2024;33(10):1381–94. doi:10.1007/s13726-024-01327-4.
67. Cheng X-W, Wu Y-X, Huang Y-T, Jiang J-R, Xu J-T, Guan J-P. Synthesis of a reactive boron-based flame retardant to enhance the flame retardancy of silk. React Funct Polym. 2020;156:104731. doi:10.1016/j.reactfunctpolym.2020.104731.
68. Shen H, Zheng X, Dong L, Huang D. Bioinspired high-strength borate cross-linked microfibrillated cellulose composite laminate with self-extinguishing flame retardance and superhydrophobicity for self-cleaning. ACS Omega. 2023;8(44):41458–68. doi:10.1021/acsomega.3c05251.
69. He S, Liu C, Chi X, Zhang Y, Yu G, Wang H, et al. Bio-inspired lightweight pulp foams with improved mechanical property and flame retardancy via borate cross-linking. Chem Eng J. 2019;371:34–42. doi:10.1016/j.cej.2019.04.018.
70. Vahabi H, Movahedifar E, Kandola BK, Saeb MR. Flame retardancy index (FRI) for polymer materials ranking. Polymers. 2023;15(11):2422. doi:10.3390/polym15112422.
71. Sharma S, Majumdar A, Butola BS. Tailoring the biodegradability of polylactic acid (PLA) based films and ramie-PLA green composites by using selective additives. Int J Biol Macromol. 2021;181:1092–103. doi:10.1016/j.ijbiomac.2021.04.108.